

# Human-Object Interaction Detection via Weak Supervision

Wiert Kilickaya,  
 kilickayamert@gmail.com  
 Arnold W.M. Smeulders  
 arnoldsmeulders@uva.nl

Visual Sensing Lab  
 University of Amsterdam  
 Amsterdam, Netherlands

## Abstract

The goal of this paper is Human-object Interaction (HO-I) detection. HO-I detection aims to find interacting human-objects regions and classify their interaction from an image. Researchers obtain significant improvement in recent years by relying on strong HO-I alignment supervision from [5]. HO-I alignment supervision pairs humans with their interacted objects, and then aligns human-object pair(s) with their interaction categories. Since collecting such annotation is expensive, in this paper, we propose to detect HO-I without alignment supervision. We instead rely on image-level supervision that only enumerates existing interactions within the image without pointing where they happen. Our paper makes three contributions: *i)* We propose Align-Former, a visual-transformer based CNN that can detect HO-I with only image-level supervision. *ii)* Align-Former is equipped with HO-I align layer, that can learn to select appropriate targets to allow detector supervision. *iii)* We evaluate Align-Former on HICO-DET [5] and V-COCO [13], and show that Align-Former outperforms existing image-level supervised HO-I detectors by a large margin (4.71% mAP improvement from 16.14% → 20.85% on HICO-DET [5]).

## Introduction

This paper strives for Human-object Interaction (HO-I) detection from an image. HO-I detection receives an astounding attention from the community recently [5, 6, 9, 10, 12, 14, 16, 18, 19, 20, 22, 24, 28], thanks to the large-scale benchmark of HICO-DET [5]. The goal is to identify the tuples of <human, object, verb, noun> from the input, where human-object is an interacting bounding box pair, and verb-noun is the interaction type, such as ride-horse.

To tackle this problem, researchers leverage strong HO-I alignment supervision, see Figure 1-(a). Annotators first draw a bounding box around all humans and objects, then align humans with the object-of-interaction (e.g., rider and horse). Finally, they align the interaction category with each human-object pairs.

However, collecting such annotation is costly<sup>1</sup>. Annotation costs time, since in a typical image there are tens of potential human-object interactors, if not hundreds. One can instead rely on image-level HO-I annotations, see Figure 1-(b). Image-level annotations enumerate existing HO-I within the image, without specifying where they occur. Image-level annotations are much faster and cheaper to collect.

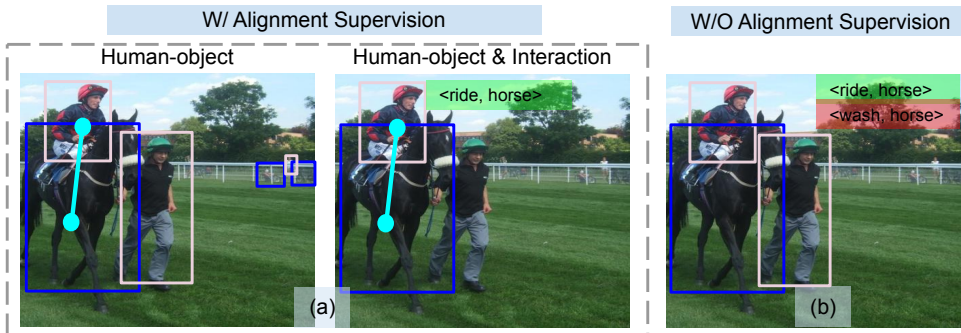


Figure 1: Alignment (left) vs. Image-level HO-I supervision (right). *a*) Alignment supervision annotates each human-objects, aligns humans to their interacting objects, then aligns human-objects to their type of interaction. *b*) Image-level supervision only lists existing interactions without pointing where they happen. Our goal is to detect HO-I *without* costly alignment supervision, by only using image-level labels.

There are few attempts to perform HO-I detection via image-level supervision [27, 60]. Initially, Zhang *et al.* [60] proposes a two-stream architecture based on Region-FCN [8], focusing on the regional appearance of subject-objects and spatial relations. Later, Kumaraswamy *et al.* [27] adapted this technique for HO-I detection, and improve it via an additional stream of human pose. These techniques yield remarkable results on HICO-DET benchmark [5] in the absence of alignment supervision. However, they are limited in three major ways: *i*) These methods isolate human-objects from their context via Region-of-Interest (RoI) pooling [10, 27], however, contextual information is crucial in understanding the interaction, *ii*) The authors propose multiple streams of context to circumvent the missing contextual information, which increases model complexity. Increased model complexity results in low performance on especially rarely represented HO-I (*i.e.*, `<ride, cow>`) as we will show. *iii*) Hand-crafted context (*i.e.*, body-pose configuration using key-points) may not be sufficient to account for the complexity of HO-I detection problem.

To that end, in this paper, we propose Align-Former, a visual-transformer-based architecture based on [9]. Align-Former is a single-stream HO-I detector that is trained end-to-end using image-level supervision only. Align-Former is equipped with a novel HO-I Align layer that learns to align a few candidate target HO-I with predictions, allowing detector supervision. The decision of alignment is based on geometric and visual priors that are crucial in HO-I detection.

This paper makes the following contributions:

- I. We propose Align-Former, an end-to-end HO-I detector that is supervised via image-level annotation.
- II. We equip Align-Former with a novel HO-I align layer, that learns to match few HO-I predictions with HO-I target(s), therefore allowing detector supervision.
- III. We evaluate Align-Former on HICO-DET [5] and V-COCO [13], and show that Align-Former outperforms competing baselines with the same level of supervision (by **4.71** mAP) on the large-scale benchmark of HICO-DET [5], especially within the low-data regime of rare categories (by **6.17** mAP).

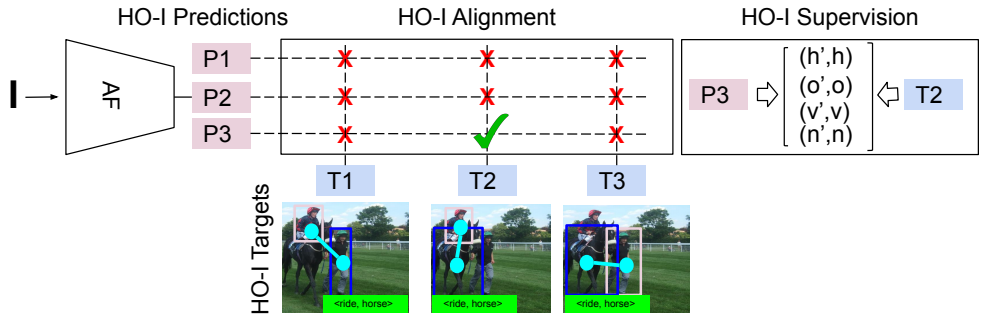


Figure 2: To perform HO-I detection via image-level supervision: *i*) Align-Former maps the input image  $I$  to HO-I predictions  $P$ . *ii*) We also prepare a set of HO-I targets by exhaustively matching human-object detections and list of interactions. *iii*) Finally, we find the least costly prediction-target pair(s) (*i.e.*,  $(T_2, P_3)$ ) which will be used for detector supervision.

## 2 Related Work

**Alignment-Supervised HO-I Detection.** In HO-I detection, the goal is to find quadruplets of  $\langle \text{human}, \text{object}, \text{verb}, \text{noun} \rangle$  where human-object are bounding boxes and verb-noun are interaction pairs like  $\langle \text{ride}, \text{horse} \rangle$ . Initially, HICO-DET authors collect more than 150k instance annotations to match humans to their interacted object, as well as to their interaction categories. Then, there has been a surge in detecting HO-I, initially via two-stage techniques [6, 9, 12, 14, 16, 24], and later by one-stage architectures [6, 10, 20, 22, 23] leveraging costly strong alignment supervision, see Figure 1-(a).

In this work, our goal is to train HO-I detectors without alignment supervision, by only relying on image-level HO-I annotations.

**HO-I Detection via Image-level Supervision.** Few works attempt to train HO-I detectors by only image-level supervision [20, 30]. Initially, Zhang *et al.* [30] proposes a two-stream architecture based on Region-FCN [8] to model the subject-object region appearance and spatial relations. Later, Kumaraswamy *et al.* [20] extends this approach via additional pose-stream. These methods operate on the isolated appearance of human-objects, neglecting the crucial context. Consequently, they supplement Region-FCN with additional streams, increasing the model size, decreasing the performance.

To circumvent this, in this work, we propose a single-stream HO-I detector based on visual-transformer [2]. Our network naturally encodes the surrounding context of human-objects thanks to self-attention [29] and learns to align few candidate HO-I targets with HO-I predictions to perform detector supervision, see Figure 2.

**Discrete Variable Sampling in Computer Vision.** In this work, we treat HO-I target alignment as a hard-valued, discrete variable sampling: Amongst all possible target-prediction pair(s), which subset(s) should be selected for detector supervision? Such decision is non-differentiable therefore ill-suited in convolutional network training. To that end, we resort to a continuous relaxation procedure named Gumbel-Softmax trick, which allows end-to-end training via discrete variables [17, 25]. Gumbel-Softmax has successfully been used to sample convolutional layers [30], filters [2] or channels [3].

In this work, we adapt Gumbel-Softmax to select the target HO-I for detector supervision.

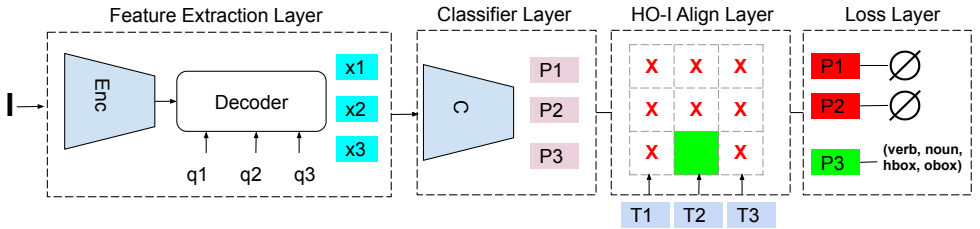


Figure 3: Align-Former consists of four main layers. **Feature Extraction Layer** is an Encoder-Decoder-based visual-transformer that extracts a set of human-object features  $x_i$  using the positional queries  $q_i$ . Then, **Classifier Layer** generates HO-I predictions  $P$  in the form of human-object bounding boxes and verb-noun classes. **HO-I Align Layer** compares HO-I predictions  $P$  with potential HO-I targets  $T$  to find few-matching pair(s) that are used for HO-I detector supervision using **Loss Layer**.

### 3 Align-Former for HO-I Detection

**Method Overview.** An overview of our technique is presented in Figure 2-3. The goal of our network  $g_\theta(\cdot)$  is to produce HO-I prediction tuples given an image  $I$  as  $I \xrightarrow{g_\theta(\cdot)} t'$ . Here, HO-I prediction is of size  $P$  and represented via  $t' = (h', o', v', n')$ , where  $(h' \in \mathbb{R}^{P \times 4}, o' \in \mathbb{R}^{P \times 4})$  are human-object bounding box predictions, and  $(v' \in \mathbb{R}^{P \times V}, n' \in \mathbb{R}^{P \times N})$  are verb-noun class predictions for  $V$  verbs and  $N$  nouns.

Then, assume we have access to a set of HO-I targets of size  $T$  with the same structure  $t = (h \in \mathbb{R}^{T \times 4}, o \in \mathbb{R}^{T \times 4}, v \in \mathbb{R}^{T \times V}, n \in \mathbb{R}^{T \times N})$ . To supervise Align-Former, we propose to minimize the following objective:

$$\min_{\theta} (A \times t, t') \quad (1)$$

where we omit  $\theta$  from now on for clarity.  $A$  is a binary matrix of size  $P \times T$  where only few entries are non-zero.  $A$  is applied separately on all tuple members, as  $A \times t = (A \times h, A \times o, A \times v, A \times n)$ . Here,  $A(i, j) = 1$  means prediction  $i$  matches (*i.e.*, aligns) with target  $j$  to use in supervision. Similarly,  $A(i, j) = 0$  indicates target  $i$  should not be used in detector supervision. To identify which target-prediction pairs should be used in detector supervision, we rely on geometric and visual priors detailed later.

Finally, replacing  $t'$  with  $g(I) = C(\text{Dec}(\text{Enc}(\text{CNN}(I)), Q))$  yields:

$$\min(A \times t, C(\text{Dec}(\text{Enc}(\text{CNN}(I)), Q)) \quad (2)$$

which is detailed in four Sections:

- **HO-I Align Layer (§3.1)** generates the alignment matrix  $A$  that pairs few HO-I prediction(s) with HO-I target(s),
- **Classification Layer (§3.2)** generates human-object bounding boxes and verb-noun classification via  $C(x)$  using human-object features  $x$ ,
- **Feature Extraction Layer (§3.3)** generates features via  $x = \text{Dec}(\text{Enc}(\text{CNN}(I)), Q)$  via positional queries  $Q$  using Encoder-Decoder architecture,
- **HO-I Loss Layer (§3.4)** computes the human-object box and verb-noun classification losses to supervise the detector with the generated HO-I targets  $t$ .

### 3.1 HO-I Align Layer

HO-I align layer consists of two sub-layers, *i*) Prior layer that judges the compatibility between all HO-I targets and predictions, *ii*) Discretization layer that binarizes the likelihood values to obtain the final hard-alignment.

#### 3.1.1 Discretization Layer

Assume we are given a scoring function  $S \in \mathbb{R}^{P \times T}$  where  $S(i, j)$  encodes how compatible HO-I prediction  $t'_i$  and HO-I target  $t_j$  matches. Our goal is to discretize this matrix to obtain the final hard-valued alignment decision.

To perform this, we discretize  $S$  such that only few members will be non-zeros. Specifically, given raw values of  $S$ , we apply the following operation:

$$A = \sigma(S + G) \geq \delta \quad (3)$$

where  $\delta = 0.5$  is the hard-threshold value,  $G$  is the Gumbel noise [14, 15] added to the matrix  $S$  for regularization, and  $\sigma(\cdot)$  is the sigmoid activation to bound  $S$  between  $[0, 1]$ . Note that Gumbel-noise is crucial to avoid any degenerate solutions like all 1s.

This operation yields the binary alignment matrix  $A \in \{0, 1\}$  where only a few entries are non-zero.

#### 3.1.2 Prior Layer

To compute the compatibility between HO-I targets & predictions, we resort to a convex combination of geometric and visual priors as  $S = \alpha_g * GP + \alpha_v * VP$ . Our intuition is that for an HO-I target to be a good candidate for detector supervision, it needs to be compatible both in terms of human-object bounding boxes (geometric) and verb-noun classes (visual).

**Geometric Prior**  $GP(\cdot)$  computes the bounding box compatibility of human-objects via  $L_1$  distance as:

$$GP = \exp\left(-\frac{\sum_{i,j} \|h'_i - h_j\| + \|o'_i - o_j\|}{\tau}\right) \quad (4)$$

where the exponential function  $\exp(\cdot)$  converts the distance values to similarity where  $\tau = 1$ .

**Visual Prior**  $VP(\cdot)$  computes how well a given target-prediction pair matches in terms of HO-I classes. Remember that our HO-I targets enumerate existing HO-I from the image in terms of verb-noun pairs. Therefore,  $VP(\cdot)$  is calculated as:

$$VP = v' * v^T + n' * n^T \quad (5)$$

where verb-predictions are of size  $v' \in \mathbb{R}^{P \times V}$  and verb-targets are of size  $v \in \mathbb{R}^{T \times V}$  for  $V$  distinct verbs. Similarly, noun-predictions are of size  $n' \in \mathbb{R}^{P \times N}$  and noun-targets  $n \in \mathbb{R}^{T \times N}$  for  $N$  distinct nouns.

## 3.2 HO-I Classification Layer

Classifier layer is responsible for generating HO-I predictions  $t'$  consisting of human-object bounding box predictions  $(h', o')$  as well as verb-noun category predictions  $(v', n')$ .

**Human-Object Bounding Box Classifiers** are two multi-layer perceptrons  $g^h(\cdot)$  and  $g^o(\cdot)$  that maps human-object features  $x$  to coordinates as  $(h', o') = (\sigma(g^h(x)), \sigma(g^o(x)))$ .

**Verb-Noun Classifiers** are also two multi-layer perceptrons as  $g^v(\cdot)$  and  $g^n(\cdot)$  that learns to map human-object features  $x$  to corresponding verb-nouns as  $(v', n') = (\sigma(g^v(x)), \sigma(g^n(x)))$ .

## 3.3 HO-I Feature Extraction Layer

Our backbone needs to encode: *i)* Object-object relations, *ii)* Relative object positions that are critical to perform HO-I alignment and detection. To that end, we implement the feature extractor as a visual-transformer based on DETR [4]. The feature extractor yields human-object features  $x \in \mathbb{R}^{P \times D}$ , and consists of three sub-layers: Backbone, Encoder and Decoder, which are detailed below.

**Backbone** ( $x = CNN(I)$ ). Backbone is a deep CNN [15] that extracts global feature maps from the input image  $I$  of size  $x \in \mathbb{R}^{H \times W \times C}$  where  $[H, W]$  are the height-width of the feature map, and  $C$  is the number of channels.

**Encoder** ( $x = Enc(x)$ ). Encoder further processes the global feature map from the backbone to increase positional and contextual information. We first reduce the number of channels from the backbone to a much smaller size via  $1 \times 1$  convolutions of  $C \times D$ . Then, the resulting feature map  $\mathbb{R}^{H \times W \times D}$  is collapsed in the spatial dimension as  $\mathbb{R}^{D \times HW}$  where each pixel becomes a "token" represented by  $D$  dimensional features. Finally, this feature undergoes a few self-attention operations via few multi-layer perceptrons, residual operations, and dropout. At each step, pixel positions are added to the feature map to retain position information.

**Decoder** ( $x = Dec(x, Q)$ ). The Decoder is a combination of self-attention and cross-attention layers, which yields the final human-object features. The Decoder takes as input the Encoder output  $x \in \mathbb{R}^{D \times HW}$  as well as fixed positional query embeddings  $Q \in \mathbb{R}^{P \times D}$ . Decoder alternates between the cross-attention between the feature map  $x$  and  $Q$ , as well as self-attention across queries. Cross-attention extracts features from the global feature maps, whereas self-attention represents object-object relations necessary for HO-I detection. Decoder is implemented as multi-layer perceptrons. Final output is  $x \in \mathbb{R}^{P \times D}$  that encodes positional and appearance-based representations of potential human-object pairs within the image.

## 3.4 HO-I Loss Layer

Our loss function ensures that the predicted human-object bounding boxes as well as the verb-noun predictions are in line with the aligned HO-I targets.

The loss function  $\mathcal{L}$  is a composite of bounding box, classification, and sparsity losses as  $\mathcal{L} = \mathcal{L}_{box} + \mathcal{L}_{class} + \mathcal{L}_{sparse}$ . Here,  $\mathcal{L}_{box}$  computes the  $L_1$  distances between human-object predictions and (aligned) targets as  $\mathcal{L}_{box} = \mathcal{L}_{human} + \mathcal{L}_{object}$ . And,  $\mathcal{L}_{class} = \mathcal{L}_{verb} + \mathcal{L}_{noun}$  are implemented via classical cross-entropy. As there can be multiple verbs for each instance, we use sigmoid activation before computing the verb loss.

**Sparsity Loss.** Finally, sparsity loss minimizes  $\mathcal{L}_{sparse} = \frac{1}{P \times T} \sum_{ij} A_{ij}$  where  $\frac{1}{P \times T}$  is a constant normalizing factor to bound the loss. This ensures the sum over all entries within the alignment matrix  $A$  is minimized, leading to only few pairs of HO-I predictions and targets to be aligned for further supervision.

**Implementation.** We set the number of predictions as  $|P| = 100$ . Our network is implemented using PyTorch [29]. Feature size  $D$  from the last layer of the Decoder is set to  $D = 256$ . Both human-object bounding box classifiers and verb and noun predictors are 2-layer perceptrons with ReLU activation in between. Initial learning rate is set to  $10^{-6}$  for the ResNet backbone and  $10^{-5}$  for the rest of the parameters. We use weight-decay to regularize the network with  $10^{-4}$ . We train the network for 150 epochs with an effective batch size of 16 over 8 GPU Titan cards. We decay the learning rate linearly with  $10^{-1}$  after epoch 100.

## 4 Experimental Setup

**Datasets.** We experiment on two large-scale standard datasets, namely HICO-DET [5] and V-COCO [13]. *i) HICO-DET* contains 38k images for training and 9.6k images for testing. Images contain 117 distinct verbs and 80 distinct nouns together, making 600  $\langle \text{verb}, \text{noun} \rangle$  pairs. For each noun, there exists a case of "no-interaction", where at least a single human and the target object is visible, even though not interacting. We only use HO-I alignment annotations for testing, and not training, since our goal is to evaluate HO-I detection via image-level supervision. *ii) V-COCO* builds upon MS-COCO [13] where the authors annotate subset of images with human-object alignments and their (inter-)action. The type of interactions is riding, reading and smiling. The dataset exhibits 2.5k images for training, 2.8k images for validation, and 4.9k images for testing.

**Metric.** We use the mean Average Precision (mAP) metric for evaluation as is the standard [5, 13]. A human-object interaction is true positive only if both humans and objects have an Intersection-over-Union with a ground-truth HO-I pair above  $> 0.50$  and they are assigned to the correct interaction categories.

**Evaluation.** *i) HICO-DET:* We use the evaluation code presented in the server [0]. We compute the mean over all three splits of full, rare, and non-rare in HICO-DET. We provide comparison on three standard splits. *Full:* All 600 categories, *Rare:* 138 categories with less than or equal to 10 training instances, *Non-Rare:* 462 categories with more than 10 training instances. *ii) V-COCO:* We use the evaluation code presented in authors' code [1]. We evaluate using three different standard scenarios. *Agent:* We report the human interactor detection performance, *Scenario-1:* We report the detection of humans and objects together, *Scenario-2:* We report the detection of humans and objects where the object predictions for object-less interactions (*i.e.*, smiling) is ignored.

**Baselines.** We compare Align-Former to *i) Weakly-supervised HO-I detectors:* PPR-FCN [6] and MX-HOI [21] that performs HO-I detection without alignment supervision. *ii) Strongly-supervised variants:* To measure the upper bound performance as a reference, we also report MX-HOI and Align-Former performance via strong alignment supervision.

## 5 HO-I Detection on HICO-DET & V-COCO

### 5.1 Comparison to The State-of-The-Art

Method	Backbone	Alignment-Supervised?	Full	Rare	Non-Rare
PPR-FCN [57]	ResNet-101	✗	15.14	10.65	16.48
MX-HOI [24]	ResNet-101	✗	16.14	12.06	17.50
Align-Former (ours)	ResNet-50	✗	<u>19.26</u>	<u>14.00</u>	<u>20.83</u>
Align-Former (ours)	ResNet-101	✗	<b>20.85</b>	<b>18.23</b>	<b>21.64</b>
MX-HOI [24]	ResNet-101	✓	17.82	12.91	19.17
Align-Former (ours)	ResNet-50	✓	25.10	17.34	27.42
Align-Former (ours)	ResNet-101	✓	27.22	20.15	29.57

Table 1: Human-Object Interaction Detection mAP on HICO-DET [5]. Our method outperforms existing techniques over all splits of full, rare, and non-rare.

**HICO-DET Results** are presented at Table 1. Overall, Align-Former outperforms the other two techniques by 3.12 mAP via ResNet-50 and 4.71 mAP via ResNet-101 on all categories. This confirms that HO-I detection benefits from the end-to-end alignment of the targets and the predictions. Our improvement is even more pronounced on the rare split via 6.17 mAP using ResNet-101, exhibiting the sample efficiency of our technique.

Method	Backbone	HICO-DET Pre-Trained?	Alignment-Supervised?	Agent	Scenario 1	Scenario 2
Align-Former	ResNet-50	✗	✗	24.63	13.90	14.15
Align-Former	ResNet-50	✓	✗	<u>27.95</u>	<u>15.52</u>	<u>16.06</u>
Align-Former	ResNet-101	✗	✗	20.00	10.44	10.79
Align-Former	ResNet-101	✓	✗	<b>30.02</b>	<b>15.82</b>	<b>16.34</b>
Align-Former	ResNet-50	✗	✓	66.78	50.20	56.42
Align-Former	ResNet-101	✗	✓	68.00	55.40	62.15

Table 2: Human-Object Interaction Detection mAP on V-COCO [14]. Even though the performance is limited when trained from scratch on V-COCO, HICO-DET pre-training yields a considerable improvement on V-COCO.

**V-COCO Results** are presented at Table 2. We only compare to our own baselines<sup>2</sup>. We evaluate two different settings. *i) Training on V-COCO from scratch:* Since the number of training images are quite limited (only 2k examples), training on V-COCO without alignment supervision yields limited accuracy on all three settings. *ii) Transfer learning from HICO-DET:* where we fine-tune a HICO-DET pre-trained model on V-COCO. In all cases, pre-training on HICO-DET helps significantly. As one of the major goal of annotation-free training is the ability to pre-train on large-scale benchmarks, we see this as a promising direction in HO-I detection with cheap image-level supervision.

We confirm that our model yields competitive performance on HICO-DET against competing benchmarks on all full, rare and non-rare splits, and showcases promising first results without alignment supervision on V-COCO, especially via transfer learning.

<sup>2</sup>Neither of the existing baselines (PPR-FCN and MX-HOI) evaluates on V-COCO. Additionally, strongly supervised stream of MX-HOI (No-Frills HO-I [24].) also is not evaluated on V-COCO

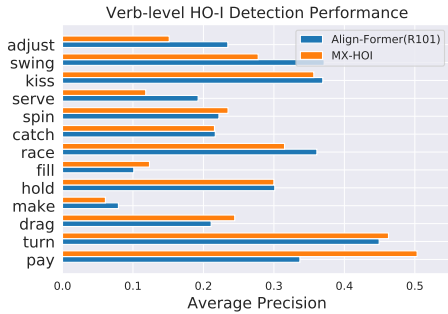


Figure 4: Verb-level Performance on HICO-DET [5]

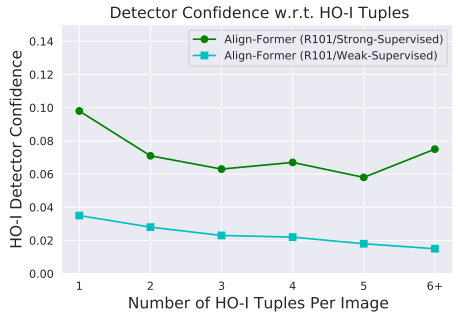


Figure 5: HO-I detector confidence w.r.t. number of HO-I tuples in an image on HICO-DET [5].

## 5.2 Further Analysis

In this section, we provide analysis to better understand the contribution of Align-Former.

**Verb-level Performance Comparison.** We visualize verb-level performance difference between weakly supervised Align-Former and MX-HOI in Figure 4. We observe that Align-Former outperforms for pose and part-driven interactions like adjust, swing or kiss, while underperforming for scene-driven interactions like pay or turn. This indicates end-to-end learning of pose-based representations is more valuable than hand-crafted pose representations as in MX-HOI. For more results, refer to our Supp. material.

**W/ vs. W/O Alignment Supervision.** To better understand the gap between strongly vs. weakly supervised HO-I detection, we provide results of MX-HOI with strong supervision on HICO-DET in Table 1 as well as strongly supervised Align-Former in both datasets (Table 1-2). Our method is flexible as it can be easily trained with strong and weak supervision with no change in architecture, whereas MX-HOI ensembles two CNNs (a weak [5] and strong [4] CNN) to do so.

We have three main findings. *i)* Weakly-supervised Align-Former outperforms strongly supervised MX-HOI on HICO-DET (Table 1), which indicates our method compensates for the lack of supervision with its representational power. *ii)* Strongly supervised Align-Former outperforms weakly supervised Align-Former on both datasets (Table 1-2). This shows Align-Former better leverages the supervision when is used, and there is a room for improvement in weakly-supervised techniques. *iii)* In Figure 5, we plot the confidence of strongly vs. weakly supervised Align-Former as a function of number of HO-I tuples in an image on HICO-DET. As can be seen, strongly-supervised variant retains its performance whereas weakly-supervised degrades in confidence, which may help explain the performance gap between the two variants of Align-Former.

**ResNet-101 vs. ResNet-50.** We implement Align-Former with ResNet-50 and 101. Even though we do not observe significant difference at the verb- or object- level, the difference is at the interaction-level. Our findings are: *i)* ResNet-101 outperforms ResNet-50 on both datasets across all settings, *ii)* Surprisingly, ResNet-101 outperforms especially on the rare split of HICO-DET, and exhibits better transferability to V-COCO, despite higher number of parameters.

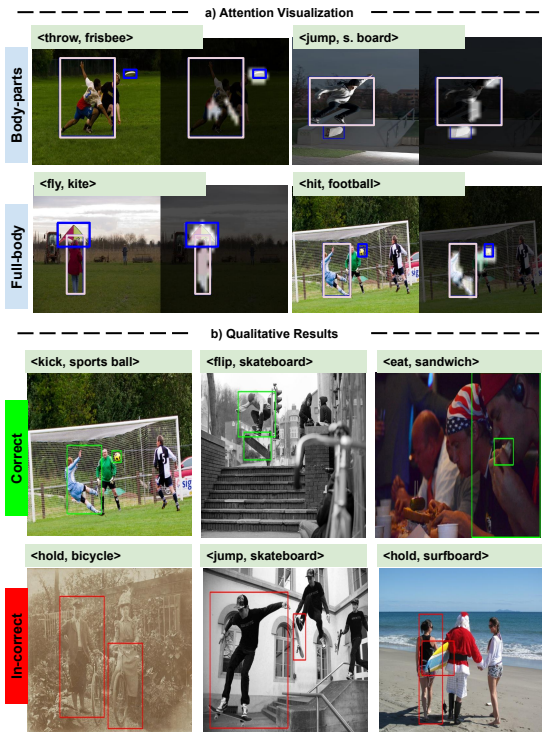


Figure 6: *a)* Attention analysis of Align-Former reveals the focus on body-part and full-body. *b)* Qualitative analysis of Align-Former reveals it can detect both dynamic and static interactions.

**Qualitative Inspection.** *i) Attention Analysis:* To understand where Align-Former is looking at to perform HO-I alignment and detection, we present the attention matrix for a set of queries from the last layer of the Decoder in Figure 6-(a). We observe that Align-Former attends on body-parts when the visual information is sufficient, and full-body when the human-object has small scale. *ii) Qualitative Results:* Finally, we visualize high-confident detection examples in Figure 6-(b). We observe that Align-Former can detect both dynamic interactions like *<kick, sports ball>* or static interactions like *<eat, sandwich>*. However, our method fails when humans can not be paired with their object of interaction, as is visualized in the bottom row.

## 6 Conclusion

This paper addressed HO-I detection from images. We proposed Align-Former, a visual-transformer based CNN that can learn to detect HO-I without alignment supervision, via image-level supervision. We equip Align-Former with HO-I align, a novel layer that learns to select correct detection targets based on geometric and visual priors. We show that Align-Former outperforms existing techniques for HO-I detection on HICO-DET especially on rare HO-I, and yields promising results on V-COCO, confirming the efficacy of our method. We hope our work inspires future research on reducing supervision in HO-I detection.

**Acknowledgements.** We are grateful for the constructive and useful feedback from all our anonymous reviewers as well as the meta reviewer, which helped us to greatly improve our manuscript.

## References

- [1] Vcoco evaluation server. In *Link*, 2015.
- [2] Hico-det evaluation server. In *Link*, 2018.
- [3] Babak Ehteshami Bejnordi, Tijmen Blankevoort, and Max Welling. Batch-shaping for learning conditional channel gated networks. *arXiv preprint*, 2019.
- [4] Nicolas Carion, Francisco Massa, Gabriel Synnaeve, Nicolas Usunier, Alexander Kirillov, and Sergey Zagoruyko. End-to-end object detection with transformers. In *ECCV*, 2020.
- [5] Yu-Wei Chao, Yunfan Liu, Xieyang Liu, Huayi Zeng, and Jia Deng. Learning to detect human-object interactions. In *WACV*, 2018.
- [6] Mingfei Chen, Yue Liao, Si Liu, Zhiyuan Chen, Fei Wang, and Chen Qian. Reformulating hoi detection as adaptive set prediction. In *CVPR*, 2021.
- [7] Zhourong Chen, Yang Li, Samy Bengio, and Si Si. You look twice: Gaternet for dynamic filter selection in cnns. In *CVPR*, 2019.
- [8] Jifeng Dai, Yi Li, Kaiming He, and Jian Sun. R-fcn: Object detection via region-based fully convolutional networks. *NeurIPS*, 2016.
- [9] Chen Gao, Yuliang Zou, and Jia-Bin Huang. ican: Instance-centric attention network for human-object interaction detection. *BMVC*, 2018.
- [10] Chen Gao, Jiarui Xu, Yuliang Zou, and Jia-Bin Huang. Drg: Dual relation graph for human-object interaction detection. In *ECCV*, 2020.
- [11] Ross Girshick. Fast r-cnn. In *ICCV*, 2015.
- [12] Georgia Gkioxari, Ross Girshick, Piotr Dollár, and Kaiming He. Detecting and recognizing human-object interactions. In *CVPR*, 2018.
- [13] Saurabh Gupta and Jitendra Malik. Visual semantic role labeling. *arXiv preprint*, 2015.
- [14] Tanmay Gupta, Alexander Schwing, and Derek Hoiem. No-frills human-object interaction detection: Factorization, appearance and layout encodings, and training techniques. *arXiv preprint*, 2018.
- [15] Kaiming He, Xiangyu Zhang, Shaoqing Ren, and Jian Sun. Deep residual learning for image recognition. In *CVPR*, 2016.
- [16] Zhi Hou, Xiaojiang Peng, Yu Qiao, and Dacheng Tao. Visual compositional learning for human-object interaction detection. In *ECCV*, 2020.

- [17] Eric Jang, Shixiang Gu, and Ben Poole. Categorical reparameterization with gumbel-softmax. *arXiv preprint*, 2016.
- [18] Mert Kilickaya and Arnold WM Smeulders. Structured visual search via composition-aware learning. In *WACV*, 2021.
- [19] Mert Kilickaya, Noureldien Hussein, Efstratios Gavves, and Arnold Smeulders. Self-selective context for interaction recognition. *arXiv preprint arXiv:2010.08750*, 2020.
- [20] Dong-Jin Kim, Xiao Sun, Jinsoo Choi, Stephen Lin, and In So Kweon. Detecting human-object interactions with action co-occurrence priors. In *ECCV*, 2020.
- [21] Suresh Kirthi Kumaraswamy, Miaoqing Shi, and Ewa Kijak. Detecting human-object interaction with mixed supervision. In *WACV*, 2021.
- [22] Yue Liao, Si Liu, Fei Wang, Yanjie Chen, Chen Qian, and Jiashi Feng. Ppdm: Parallel point detection and matching for real-time human-object interaction detection. In *CVPR*, 2020.
- [23] Tsung-Yi Lin, Michael Maire, Serge Belongie, James Hays, Pietro Perona, Deva Ramanan, Piotr Dollár, and C Lawrence Zitnick. Microsoft coco: Common objects in context. In *ECCV*, 2014.
- [24] Yang Liu, Qingchao Chen, and Andrew Zisserman. Amplifying key cues for human-object-interaction detection. In *ECCV*, 2020.
- [25] Chris J Maddison, Andriy Mnih, and Yee Whye Teh. The concrete distribution: A continuous relaxation of discrete random variables. *arXiv preprint*, 2016.
- [26] Adam Paszke, Sam Gross, Soumith Chintala, Gregory Chanan, Edward Yang, Zachary DeVito, Zeming Lin, Alban Desmaison, Luca Antiga, and Adam Lerer. Automatic differentiation in pytorch. 2017.
- [27] Shaoqing Ren, Kaiming He, Ross Girshick, and Jian Sun. Faster r-cnn: Towards real-time object detection with region proposal networks. In *NeurIPS*, 2015.
- [28] Masato Tamura, Hiroki Ohashi, and Tomoaki Yoshinaga. Qpic: Query-based pairwise human-object interaction detection with image-wide contextual information. In *CVPR*, 2021.
- [29] Ashish Vaswani, Noam Shazeer, Niki Parmar, Jakob Uszkoreit, Llion Jones, Aidan N Gomez, Łukasz Kaiser, and Illia Polosukhin. Attention is all you need. In *NeurIPS*, 2017.
- [30] Andreas Veit and Serge Belongie. Convolutional networks with adaptive inference graphs. In *ECCV*, 2018.
- [31] Hanwang Zhang, Zawlin Kyaw, Jinyang Yu, and Shih-Fu Chang. Ppr-fcn: Weakly supervised visual relation detection via parallel pairwise r-fcn. In *ICCV*, 2017.